ACS APPLIED MATERIALS & INTERFACES

Research Article

www.acsami.org

Elemental Mapping of Interfacial Layers at the Cathode of Organic Solar Cells

Gopal K. Mor,[†] Thinh P. Le,[†] Kiarash Vakhshouri,[†] Derek R. Kozub,[†] and Enrique D. Gomez*[,†,‡]

[†]Department of Chemical Engineering, The Pennsylvania State University, University Park, Pennsylvania 16802, United States

[‡]Materials Research Institute, The Pennsylvania State University, University Park, Pennsylvania 16802, United States

Supporting Information

ABSTRACT: One of the limitations in understanding the performance of organic solar cells has been the unclear picture of morphology and interfacial layers developed at the active layer/cathode interface. Here, by utilizing the shadow-Focused Ion Beam technique to enable energy-filtered transmission electron microscopy imaging in conjunction with X-ray photoelectron spectroscopy (XPS) experiments, we examine the cross-section of polythiophene/fullerene solar cells to characterize interfacial layers near the semiconductor-cathode interface. Elemental mapping reveals that localization of fullerene to the anode interface leads to low fill factors and S-shaped current−voltage characteristics. Furthermore, the combination of elemental mapping and XPS depth profiles of devices demonstrate oxidation of the aluminum cathode at the active layer interface for devices without S-shaped characteristics and fill factors of 0.6. The presence of a thin dielectric at the semiconductor-cathode interface could minimize electronic barriers for charge extraction by preventing interfacial charge reorganization and band-bending.

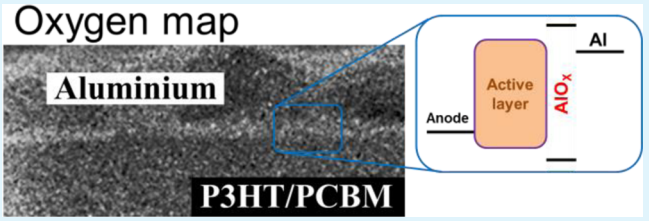

KEYWORDS: *energy-filtered TEM, organic photovoltaics, contacts, FIB, P3HT, PCBM*

INTRODUCTION

The tremendous recent progress in the photoconversion efficiencies of solution-processed organic solar cells brings these devices closer to commercialization.[1−3] Among other aspects, continued development hinges on creating contacts with minimal loses at the cathode and anode electrodes. For example, various interfacial layers at the cathode surface have been demonstrated to enhance performance of organic photovoltaics. Low work function metals which are too unstable or possess conductivities which are too low for an electrode material have been utilized as interfacial layers, including Ca and Ba.[4] Other semiconductors with low work functions, such as ZnO,[5] TiOx,[6,7] and insulators, such as LiF,[8] have also been employed as interface modifiers. Furthermore, thin layers of conjugated polyelectrolytes[9] and insulating polymers such as poly(ethylene oxide)[10] or poly(ethylenimine)[11] at the cathode surface can enhance the performance of organic photovoltaics.

Effective cathodic contacts in donor/acceptor solar cells are made with low work function electrodes. In principle, materials with work functions near 4 eV can minimize transport barriers for charge extraction from high electron affinity acceptors in the active layer, such as fullerene, by minimizing band-bending at the electrode-semiconductor interface. Nevertheless, polarization and charge reorganization or transfer can lead to vacuum level shifts that are understood in terms of interfacial dipoles at contacts and barriers for charge extraction.[12,13] For example, previous work has examined barriers for charge extraction between ITO electrodes and the active layer, where ITO anodes were modified with several self-assembled monolayers (SAMs). By utilizing both electron-donating and electron-withdrawing SAMs, the work function of the anode was modified between 4 and 5.5 eV. Nevertheless, the interfacial barriers for hole extraction at the anode from poly(3-hexylthiophene)/[6,6]-phenyl-C_{61}-butyric acid methyl ester (P3HT/PCBM) active layers, as measured by ultraviolet photoemission spectroscopy, were invariant at approximately 0.5 eV.[14] Thus, the specific value of the electrode work function is often not as important for charge extraction as interfacial phenomena which are responsible for ubiquitous electronic barriers at contacts.

One complication to the interpretation of the electrical properties of organic diodes is that the composition of active layers and electrodes can vary significantly near interfaces due to the spontaneous creation of surface wetting layers or diffusion of oxygen or water.[15−19] For example, Wang et al. has demonstrated that compositional interfacial layers in P3HT/PCBM active layers can have an effect on device performance in an asymmetric fashion in devices.[20] P3HT does not appear to block electron conduction while PCBM is very effective at blocking hole transport. These studies, however, rely on characterizing interfacial layers at air interfaces or anodic buried interfaces through delamination; few studies have examined the cross-section of actual devices.[21] Notably, experiments utilizing

Received: July 1, 2014
Accepted: October 27, 2014
Published: October 27, 2014

time-of-flight secondary ion mass spectrometry have examined the oxidation within organic solar cells by isotopically labeled water and oxygen to demonstrate that oxygen diffuses through the aluminum electrode and creates aluminum oxide, which is insulating and can severely degrade device performance.[22−24]

Here, we examine the cathode interface using energy-filtered transmission electron microscopy and X-ray photoelectron spectroscopy (XPS) in solar cells composed of poly(3-hexylthiophene-2,5-diyl) (P3HT)/[6,6]-phenyl C_{71}-butyric acid methyl ester (PCBM) mixtures as the active layer. We find that AlO_x forms preferentially at the cathode interface, even when devices are fabricated in an inert environment and exhibit high fill factors (ca. 0.6). Furthermore, a slight enrichment of fullerene may also exist at the cathode electrode. We hypothesize that the presence of AlO_x could aid in charge extraction, by providing a thin dielectric layer in between the electrode and active layer, which prevents the formation of interfacial electronic barriers for charge extraction.

RESULTS AND DISCUSSION

Organic photovoltaic devices can often exhibit an "S" shaped curve in the current−voltage (J−V) characteristics. In order to examine this phenomenon, we deposited solutions of P3HT/PCBM mixtures and allowed them to soak the substrate for approximately 3 min prior to turning on the spin-coater. Figure 1 shows the device characteristics of such a device, where a current−voltage curve demonstrates a kink as the open-circuit voltage (V_{OC}) is approached. The average efficiency over six devices is 0.95 ± 0.09%, with a short-circuit current of 8.4 ± 0.9 mA/cm^2, open-circuit voltage of 0.50 ± 0.02, and fill factor of 0.23 ± 0.02. The photocurrent drops dramatically as the load increases, suggesting the presence of a blocking layer or a reverse diode connected in series with the donor/acceptor heterojunction.[25−30]

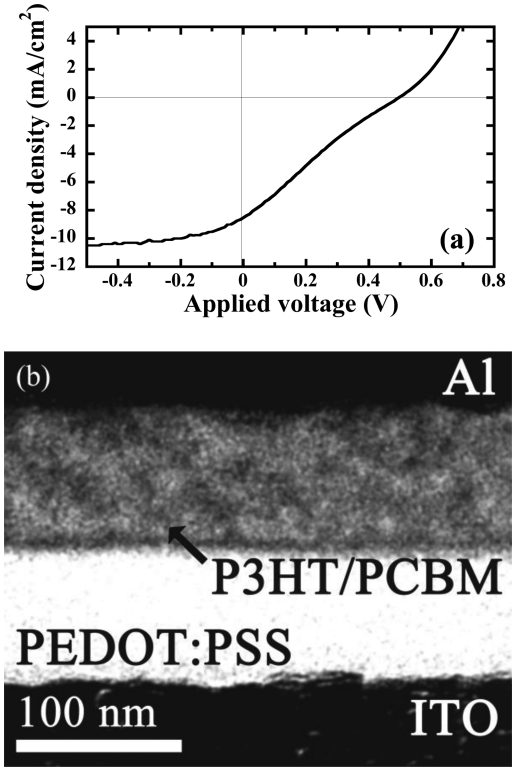

Figure 1. (a) Current−voltage characteristics of a P3HT/PCBM solar cell exhibiting an inflection point and a poor fill factor. The device characteristics are representative of six devices. (b) Sulfur elemental map of the cross-section of the device shown in part a. A thin layer of PCBM (dark stripe) is apparent at the PEDOT:PSS interface.

We can examine the presence of stratification or wetting layers by cross-sectioning devices. The presence of hard and soft layers, however, makes cross-sectioning through standard techniques such as ultramicrotomy challenging. Instead, we utilize the Focused Ion Beam in a "shadow" configuration. The shadow-FIB technique, developed by Kim and Minor,[31,32] maintains the ion beam perpendicular to the sample at all times to minimize ion implantation and damage to the sample. Figure 1b shows a sulfur elemental map taken of a cross-section created using the shadow-FIB method. The light regions correspond to the presence of sulfur and therefore P3HT. The microstructure of the P3HT/PCBM film is visible within the active layer, and consistent with top-view sulfur elemental maps previously reported.[33−35] In addition, a dark band is visible at the PEDOT:PSS interface, indicative of a PCBM wetting layer. The presence of PCBM at the anode can prevent hole extraction by providing a barrier for charge extraction.[20]

We now examine a solar cell fabricated without a holding time prior to spin-coating such that no "S" shape behavior was apparent in the device performance. As a result, the average power conversion efficiency for devices is 3.6 ± 0.3% and the average fill factor is 0.61 ± 0.02 (Figure S1 of the Supporting Information). The device was annealed at 160 °C for 10 min in order to optimize performance. All devices were fabricated in a N_2 glovebox equipped with an integrated spin-coater and evaporator. The oxygen elemental map of a device cross-section whose performance characteristics are shown in Figure S1 of the Supporting Information is shown in Figure 2a. The presence of oxygen enrichment at the interface between Al and the P3HT/PCBM active layer is apparent. Figure 2b shows the

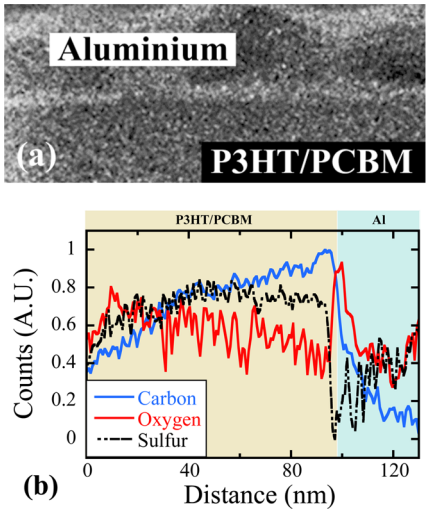

Figure 2. (a) Oxygen elemental map of the cross-section of a P3HT/PCBM device annealed at 165 °C for 10 min. The aluminum-P3HT/PCBM interface shows an enrichment of oxygen. (b) Normalized counts obtained from oxygen, carbon, and sulfur maps as a function of distance away from the PEDOT:PSS interface. Colored regions denote the active layer (P3HT/PCBM, ca. 100 nm thick) and the Al cathode. We attribute the small peak in the carbon map at ∼100 nm to fullerene aggregation near the Al interface and the large peak in the oxygen map at the Al interface to the presence of AlO_x.

intensities for carbon, oxygen, and sulfur elemental maps generated from a cross-section of the same P3HT/PCBM device shown in Figure 2a. The carbon and sulfur counts drop suddenly at the aluminum interface as expected. Nevertheless, the cathode interface is not perfectly sharp, likely due to the surface roughness of P3HT/PCBM films. Although the carbon counts continuously decrease into the Al layer, the sulfur counts increase. Because the counts from elemental maps are a product of the thickness and elemental composition, we attribute the increase in the sulfur counts in the aluminum layer (ca. 120 nm in Figure 2b) to an artifact from nonuniform sample preparation, such that the TEM sample is thicker near the cathode. Indeed, the carbon counts show a slope within the active layer, suggesting that the TEM sample is thicker near the cathode, although no slope is apparent in the carbon counts within the Al layer.

Our discussion of the elemental map data focuses on the features apparent near the cathode. Some enrichment of carbon is apparent near the cathode interface, suggesting that PCBM preferentially wets the Al surface. Furthermore, an oxygen peak at the cathode interface is visible, corroborating the profile obtained from the carbon map. The location and breadth of the peak, however, appears slightly shifted toward the Al electrode. A possible explanation for the presence of oxygen at the Al interface is that AlO_x is present due to oxidation of the cathode.

We utilized XPS to examine the cathode interface in model structures. We fabricated stacks composed of Si(with native oxide)/PEDOT:PSS substrates followed by P3HT/PCBM films with Al on top. By sputter etching with an Ar^+ ion gun within the XPS, we collected depth profiles of our films. Figure 3 shows the XPS spectra as a function of sputter time (depth), where spectra is acquired every 30 s. Data is shown as a function of time from back to front. Oxygen is clearly visible at the top of the film, due to oxidation of the Al during transportation of the sample from the N_2 glovebox to the XPS. The oxygen peak decreases significantly as we probe deeper into the film, but then increases again as we approach the organic film (as indicated by the rise in the carbon 1s and sulfur 2p intensity). Furthermore, the Al spectra show the presence of two peaks. The lower energy peak near 73 eV corresponds to Al^0, while the higher energy peak near 74 eV corresponds to Al^{3+}.[36] Thus, Figures 2 and 3 suggest that AlO_x is present at the interface between the active layer and cathode in P3HT/PCBM solar cells.

The presence of AlO_x at the cathode interface could be due to various reasons. The oxygen in the ester group of PCBM could react with Al, water, or oxygen trapped in PEDOT:PSS could diffuse through the active layer and oxidize the Al surface, oxygen present in the glovebox atmosphere could oxidize the cathode, and residual oxygen or water could diffuse out of the active layer to react with the Al electrode. As shown below, we demonstrate that oxygen or water within P3HT/PCBM mixtures can diffuse out of the active layer without exposure to ambient and form an AlO_x layer at the cathode interface.

Figure 4 shows atomic concentration profiles obtained from XPS data for films containing P3HT/PCBM, P3HT, or PCBM

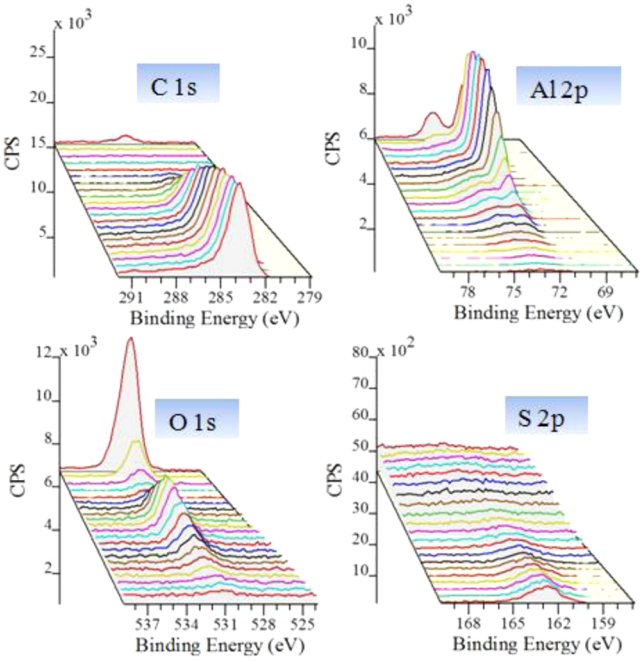

Figure 3. XPS depth profiles of P3HT/PCBM films with Al on top. C 1*s*, O 1*s*, S 2*p* and Al 2*p* regions are shown. Data is acquired every 30 s during depth profiling of the film. Spectra acquired at earliest times (top of film) are shown in the back. In the Al spectra, the growth of a peak near 75−76 eV indicative of Al^{3+} (AlO_x) is observed at the top surface and near the active layer/cathode interface.

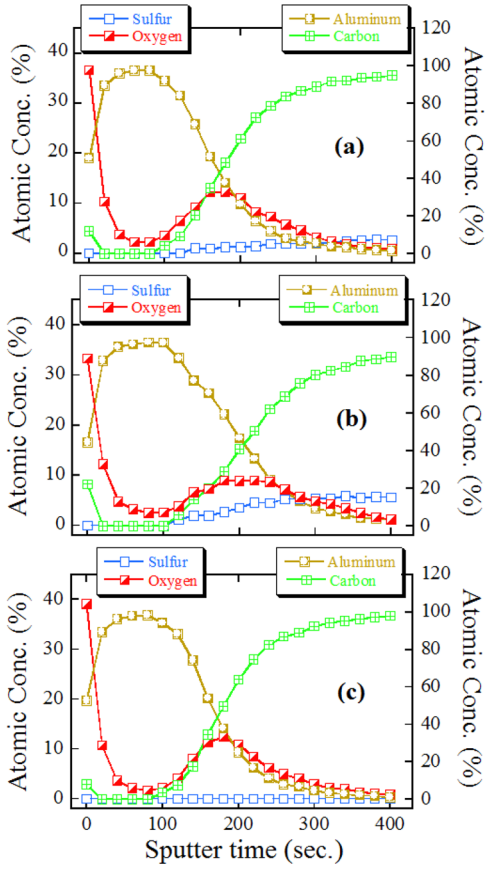

Figure 4. Concentrations of C, O, S, Al elements as a function of sputter time (depth profiling) in the XPS. Data is shown for (a) P3HT/PCBM films with Al on top, (b) neat P3HT with Al, and (c) neat PCBM with Al. Layers were deposited on Si/PEDOT:PSS substrates. Samples were annealed after Al deposition at 160 °C for 10 min. The presence of oxygen at the active layer-Al interface is clear in all samples.

films in between Si/PEDOT:PSS and Al electrodes. Films stacks are fabricated to closely simulate the device architecture and all samples are annealed at 160 °C for 10 min, similarly to solar cells. XPS spectra for test structures containing only P3HT or PCBM as the active layer are shown in Figure S2 and Figure S3 of the Supporting Information. Oxygen is present at the top interface (sputter time = 0) due to oxidation of Al when the films are briefly exposed to air prior to loading the sample into the XPS instrument. As the sputter time increases, spectra are representative of regions deeper into the film, and the Al concentration decreases rapidly near 200 s while the carbon concentration increases. The presence of oxygen at the interface between Al and P3HT/PCBM is apparent for all three samples, indicating that P3HT and PCBM contribute roughly equally to the formation of AlO_x. As shown in Figure S4 of the Supporting Information, removing PEDOT:PSS from the film stack does not significantly affect the presence of the oxygen peak at the Al interface.

Figure 5 shows XPS depth profiles of films composed of aluminum deposited on Si. Oxygen is present at the top of the

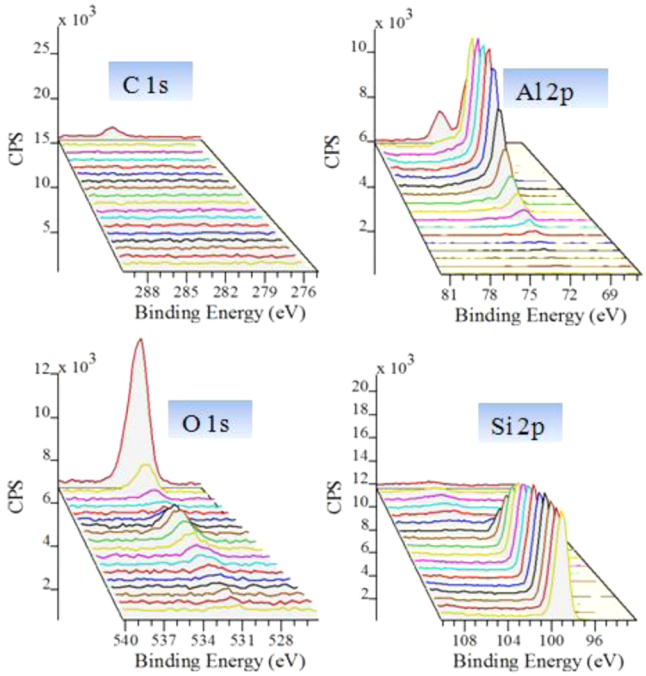

Figure 5. XPS depth profiles of Si/Al. XPS spectra were recorded for C 1s, Al 2p, O 1s, and Si 2p every 30 s during sputter etching of the film. Spectra acquired at earliest times (top of film) are shown in the back. The absence of the Al^{3+} peak at the Al/Si interface demonstrates that the formation of AlO_x at organic interfaces shown in Figures 2−4 is not due to oxygen or water contamination from the glovebox atmosphere.

film due to oxidation of Al, and some oxygen is also present at the Si surface due to the native oxide layer. Al^{3+}, however, is clearly suppressed with respect to film stacks containing an organic layer. Thus, we conclude that the presence of AlO_x at the interface between Al and P3HT/PCBM apparent from Figures 2−4 is not due to trace oxygen or water in the glovebox atmosphere, where all device fabrication took place. Figure 6 compares the ratio of the intensity of the Al^{3+} and Al^0 peak for the various film stacks. It is apparent that the presence of Al^{3+} is clear in all films containing organic layers, regardless of whether

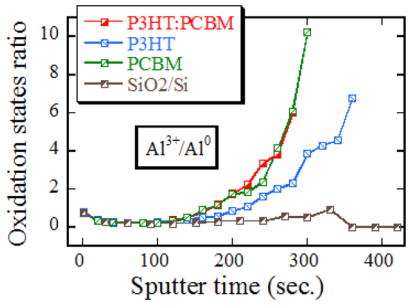

Figure 6. Ratio of the area under the Al^{3+} and Al^0 peaks in XPS data plotted as a function of sputter time (depth profiling) for four film stacks: Si/PEDOT:PSS/P3HT:PCBM/Al, Si/PEDOT:PSS/P3HT/Al, Si/PEDOT:PSS/PCBM/Al, and Si/Al films. The lack of Al^{3+} in samples composed of Si(native oxide)/Al suggests that the formation of AlO_x is due to residual oxygen or water in both P3HT and PCBM.

the film is a mixture of P3HT and PCBM or neat P3HT or PCBM.

Thus, we hypothesize that the formation of AlO_x at the cathode interface is due to trace amounts of oxygen or water, which is present in either P3HT, PCBM, or the solvents utilized to make the spin-casting solutions. Our protocols minimize the exposure to ambient, similarly to other published device fabrication methodologies.[37−39] Materials and anhydrous solvents are all stored in an N_2 glovebox, all solutions are made in the glovebox, and films are spun-cast or thermally evaporated within the glovebox. The only exposure to ambient takes place during the weighing of the materials, prior to dissolution in anhydrous solvents within the glovebox. Thus, residual oxygen or water is either strongly absorbed or trapped within the materials or is quickly absorbed during the brief exposure, ca. 15 min, of the solids to air (films are never exposed to air).

The presence of an AlO_x layer at the cathode interface could be helpful toward device performance. We speculate that adding a dielectric layer at the cathodic contact could reduce band-bending near the interface and prevent the formation of interfacial electronic barriers. The dielectric layer would prevent polarization or charge transfer/reorganization between the active layer and semiconductor, because of the strong reduction in electronic coupling or interactions between P3HT/PCBM and the cathode. Thus, if the dielectric layer is thin enough to allow charge tunneling through the AlO_x layer, the oxidation of Al may prevent the formation of interfacial states and barriers for charge extraction. Indeed, when the pressure in the evaporator is very low, near 10^{-10} Torr (compared to our evaporator operating at 10^{-6} Torr), the open-circuit of P3HT/PCBM solar cells is significantly lower, near 0.4 V, than the 0.6 V reported here.[4] We predict that devices where aluminum is deposited at ultrahigh vacuum (ca. 10^{-10} Torr) do not exhibit AlO_x layers at the electrode interface and therefore depend more strongly on thin cathodic layers, such as LiF, to extract electrons. For such devices, we also predict that a thin layer of AlO_x, deposited perhaps through atomic layer deposition or plasma-enhanced atomic layer deposition,[40] could lead to an improvement in device performance.

CONCLUSIONS

In summary, we have utilized the combination of the shadow-FIB, elemental mapping through energy-filtered TEM, and XPS depth profiling to characterize the cathode interface in P3HT/PCBM solar cells. We find that a thin layer of AlO_x is present at

the active layer-cathode interface, even for devices with fill factors of 0.6. The oxygen source in devices appears to be the active layer, where trace oxygen and water diffuse from the organic film to the Al surface. We hypothesize that the presence of AlO_x at the cathode contact can suppress the formation of interfacial electronic barriers by placing a dielectric layer at the active layer-Al interface.

EXPERIMENTAL PROCEDURES

Devices were fabricated as previously described.[34,41] Briefly, patterned ITO-coated glass was cleaned using a nonionic surfactant (Aquet) and then thoroughly rinsed with ultrapure water (18.2 MΩ-cm). Substrates were dried with filtered compressed air and then sonicated in acetone and 2-propanol for 10 min each. After drying with filtered compressed air, the slides were place in an oven at 80 °C for 10 min. The final cleaning step for the substrates is UV−ozone exposure for 15 min.

A thin PEDOT:PSS (Clevios P, H. C. Starck) layer was spin coated at 4000 rpm for 2 min and subsequently baked at 160 °C for 10 min in air. These coated slides were immediately transferred into an N_2 glovebox (M-Braun). P3HT (95.9% H-T regioregular, M_n = 51 kg/mol, polydisperity = 2, Merck) and PCBM (C70PCBM, >99.5%, Nano-C) were weighed together in a cleaned and dried amber-colored vial. After transferring the materials into the glovebox, anhydrous chlorobenzene (Sigma-Aldrich) was added and allowed to stir overnight at 40−45 °C. The concentration of the solution was 16 mg/mL with P3HT/PCBM present in a ratio of 1 to 0.9. After putting 250 μL of the P3HT/PCBM solution on PEDOT:PSS-coated ITO slides, wetting was allowed at 50 rpm for 60 s before spin coating at 600 rpm for 60 s.

Films deposited on ITO slides were then transferred into an evaporation chamber integrated with the glovebox for cathode deposition. Aluminum was deposited on samples through shadow masks, such that six subcells with area of 0.162 cm^2 were created per one square inch substrate. Aluminum was evaporated at 5×10^{-6} mbar with an initial deposition rate of 0.3 to 0.4 Å/s for 20 min. The deposition rate was then increased to 1−1.5 Å/s until a final aluminum thickness of 60 nm was achieved. Finally, devices were annealed at 160 °C for 10 min in the dark.

To prepare samples for FIB work, a small sharp triangular piece was cut from devices using a scribe. The shard was transferred onto copper grids, which have a notch to support the sample. The orientation of the sample was such that cross sections of devices are parallel to the grid plane and the tip (region of interest) is in the center of the grid. Finally, carbon paste is applied over the exposed glass to avoid charging during FIB work. The shadow-FIB method[32] maintains the Ga^+ ion beam perpendicular to the substrate by dictating that milling takes place from the back side (substrate side) and perpendicular to the region of interest for TEM imaging. Thus, the sample receives Ga^+ ions at a glancing geometry and never directly. FIB work was performed using a FIB/SEM Quanta 200 with an ion beam current in the range from 30 to 50 pA to achieve thicknesses of 80−100 nm.

Energy-filtered TEM measurements were performed at the National Center for Electron Microscopy, Lawrence Berkeley National Laboratory, on a Zeiss LIBRA 200MC. Bright field images, thickness maps, and elemental maps were captured. Thickness maps for each sample were taken to check the uniformity of the film thickness. Elemental maps were generated through the standard three-window method.

Identification of elements and their chemical state near the interfacial region was performed by depth profiling using an XPS (Kratos) equipped with a monochromatic Al K X-ray source (1486.6 eV). Si wafers (with native oxide surfaces) were used as substrates for all samples. Charge neutralization was employed. Compositions were calculated from the XPS spectra for Al 2p, O 1s, C 1s, and S 2p regions after background subtraction using CasaXPS software (Casa Software Ltd., Teignmouth, U.K.).

ASSOCIATED CONTENT

Supporting Information

Device testing, device characteristics, and XPS results. This material is available free of charge via the Internet at http://pubs.acs.org.

AUTHOR INFORMATION

Corresponding Author

*E-mail: edg12@psu.edu.

Notes

The authors declare no competing financial interest.

ACKNOWLEDGMENTS

The authors gratefully acknowledge the help of Tim Tighe from the Materials Characterization Lab at the Materials Institute of Penn State for XPS measurements. Financial support of this work through the National Science Foundation (Award no. CBET-1067470) is acknowledged. The authors acknowledge support of the National Center for Electron Microscopy, Lawrence Berkeley National Laboratory, by the U.S. Department of Energy under Contract No. DE-AC02-05CH11231.

REFERENCES

(1) Liang, Y.; Xu, Z.; Xia, J.; Tsai, S.-T.; Wu, Y.; Li, G.; Ray, C.; Yu, L. For the Bright Future—Bulk Heterojunction Polymer Solar Cells with Power Conversion Efficiency of 7.4%. *Adv. Mater.* **2010**, *22*, E135−E138.

(2) You, J. B.; Dou, L. T.; Yoshimura, K.; Kato, T.; Ohya, K.; Moriarty, T.; Emery, K.; Chen, C. C.; Gao, J.; Li, G.; Yang, Y. A Polymer Tandem Solar Cell with 10.6% Power Conversion Efficiency. *Nat. Commun.* **2013**, *4*, 1446.

(3) Chen, K.-S.; Yip, H.-L.; Salinas, J.-F.; Xu, Y.-X.; Chueh, C.-C.; Jen, A. K. Y. Strong Photocurrent Enhancements in Highly Efficient Flexible Organic Solar Cells by Adopting a Microcavity Configuration. *Adv. Mater.* **2014**, *26*, 3349−3354.

(4) Reese, M. O.; White, M. S.; Rumbles, G.; Ginley, D. S.; Shaheen, S. E. Optimal Negative Electrodes for Poly(3-hexylthiophene)/[6,6]-Phenyl C61-Butyric Acid Methyl Ester Bulk Heterojunction Photovoltaic Devices. *Appl. Phys. Lett.* **2008**, *92*, 053307.

(5) Hau, S. K.; Yip, H. L.; Baek, N. S.; Zou, J. Y.; O'Malley, K.; Jen, A. K. Y. Air-Stable Inverted Flexible Polymer Solar Cells using Zinc Oxide Nanoparticles as an Electron Selective Layer. *Appl. Phys. Lett.* **2008**, *92*, 253301.

(6) Hau, S. K.; Yip, H. L.; Acton, O.; Baek, N. S.; Ma, H.; Jen, A. K. Y. Interfacial Modification to Improve Inverted Polymer Solar Cells. *J. Mater. Chem.* **2008**, *18*, 5113−5119.

(7) Waldauf, C.; Morana, M.; Denk, P.; Schilinsky, P.; Coakley, K.; Choulis, S. A.; Brabec, C. J. Highly Efficient Inverted Organic Photovoltaics Using Solution based Titanium Oxide as Electron Selective Contact. *Appl. Phys. Lett.* **2006**, *89*, 233517.

(8) Brabec, C. J.; Shaheen, S. E.; Winder, C.; Sariciftci, N. S.; Denk, P. Effect of LiF/Metal Electrodes on the Performance of Plastic Solar Cells. *Appl. Phys. Lett.* **2002**, *80*, 1288−1290.

(9) Seo, J. H.; Gutacker, A.; Sun, Y. M.; Wu, H. B.; Huang, F.; Cao, Y.; Scherf, U.; Heeger, A. J.; Bazan, G. C. Improved High-Efficiency Organic Solar Cells via Incorporation of a Conjugated Polyelectrolyte Interlayer. *J. Am. Chem. Soc.* **2011**, *133*, 8416−8419.

(10) Jung, J. W.; Jo, J. W.; Jo, W. H. Enhanced Performance and Air Stability of Polymer Solar Cells by Formation of a Self-Assembled Buffer Layer from Fullerene-End-Capped Poly(ethylene glycol). *Adv. Mater.* **2011**, *23*, 1782−1787.

(11) Zhou, Y. H.; Fuentes-Hernandez, C.; Shim, J.; Meyer, J.; Giordano, A. J.; Li, H.; Winget, P.; Papadopoulos, T.; Cheun, H.; Kim, J.; Fenoll, M.; Dindar, A.; Haske, W.; Najafabadi, E.; Khan, T. M.; Sojoudi, H.; Barlow, S.; Graham, S.; Bredas, J. L.; Marder, S. R.; Kahn,

A.; Kippelen, B. A Universal Method to Produce Low-Work Function Electrodes for Organic Electronics. *Science* **2012**, *336*, 327−332.
(12) Hwang, J.; Wan, A.; Kahn, A. Energetics of Metal−Organic Interfaces: New Experiments and Assessment of the Field. *Mater. Sci. Eng., R* **2009**, *64*, 1−31.
(13) Cahen, D.; Kahn, A. Electron Energetics at Surfaces and Interfaces: Concepts and Experiments. *Adv. Mater.* **2003**, *15*, 271−277.
(14) Wang, H.; Gomez, E. D.; Guan, Z.; Jaye, C.; Toney, M. F.; Fischer, D. A.; Kahn, A.; Loo, Y.-L. Tuning Contact Recombination and Open-Circuit Voltage in Polymer Solar Cells via Self-Assembled Monolayer Adsorption at the Organic−Metal Oxide Interface. *J. Phys. Chem. C* **2013**, *117*, 20474−20484.
(15) Mauger, S. A.; Chang, L. L.; Friedrich, S.; Rochester, C. W.; Huang, D. M.; Wang, P.; Moule, A. J. Self-Assembly of Selective Interfaces in Organic Photovoltaics. *Adv. Funct. Mater.* **2013**, *23*, 1935−1946.
(16) Campoy-Quiles, M.; Ferenczi, T.; Agostinelli, T.; Etchegoin, P. G.; Kim, Y.; Anthopoulos, T. D.; Stavrinou, P. N.; Bradley, D. D. C.; Nelson, J. Morphology Evolution via Self-Organization and Lateral and Vertical Diffusion in Polymer/Fullerene Solar Cell Blends. *Nat. Mater.* **2008**, *7*, 158−164.
(17) Xu, Z.; Chen, L. M.; Yang, G. W.; Huang, C. H.; Hou, J. H.; Wu, Y.; Li, G.; Hsu, C. S.; Yang, Y. Vertical Phase Separation in Poly(3-hexylthiophene)/Fullerene Derivative Blends and its Advantage for Inverted Structure Solar Cells. *Adv. Funct. Mater.* **2009**, *19*, 1227−1234.
(18) Felicissimo, M. P.; Jarzab, D.; Gorgoi, M.; Forster, M.; Scherf, U.; Scharber, M. C.; Svensson, S.; Rudolf, P.; Loi, M. A. Determination of Vertical Phase Separation in a Polyfluorene Copolymer/Fullerene Derivative Solar Cell Blend by X-ray Photoelectron Spectroscopy. *J. Mater. Chem.* **2009**, *19*, 4899−4901.
(19) Germack, D. S.; Chan, C. K.; Hamadani, B. H.; Richter, L. J.; Fischer, D. A.; Gundlach, D. J.; DeLongchamp, D. M. Substrate-Dependent Interface Composition and Charge Transport in Films for Organic Photovoltaics. *Appl. Phys. Lett.* **2009**, *94*, 233303.
(20) Wang, H.; Shah, M.; Ganesan, V.; Chabinyc, M. L.; Loo, Y. L. Tail State-Assisted Charge Injection and Recombination at the Electron-Collecting Interface of P3HT:PCBM Bulk-Heterojunction Polymer Solar Cells. *Adv. Energy Mater.* **2012**, *2*, 1447−1455.
(21) Chen, D.; Liu, F.; Wang, C.; Nakahara, A.; Russell, T. P. Bulk Heterojunction Photovoltaic Active Layers via Bilayer Interdiffusion. *Nano Lett.* **2011**, *11*, 2071−2078.
(22) Norrman, K.; Krebs, F. C. Lifetimes of Organic Photovoltaics: Using TOF-SIMS and $^{18}O_2$ Isotopic Labelling to Characterise Chemical Degradation Mechanisms. *Sol. Energy Mater. Sol. Cells* **2006**, *90*, 213−227.
(23) Norrman, K.; Larsen, N. B.; Krebs, F. C. Lifetimes of Organic Photovoltaics: Combining Chemical and Physical Characterisation Techniques to Study Degradation Mechanisms. *Sol. Energy Mater. Sol. Cells* **2006**, *90*, 2793−2814.
(24) Jørgensen, M.; Norrman, K.; Krebs, F. C. Stability/Degradation of Polymer Solar Cells. *Sol. Energy Mater. Sol. Cells* **2008**, *92*, 686−714.
(25) Wagner, J.; Gruber, M.; Wilke, A.; Tanaka, Y.; Topczak, K.; Steindamm, A.; Hormann, U.; Opitz, A.; Nakayama, Y.; Ishii, H.; Pflaum, J.; Koch, N.; Brutting, W. Identification of Different Origins for S-Shaped Current Voltage Characteristics in Planar Heterojunction Organic Solar Cells. *J. Appl. Phys.* **2012**, *111*, 054509.
(26) Ecker, B.; Egelhaaf, H. J.; Steim, R.; Parisi, J.; von Hauff, E. Understanding S-Shaped Current−Voltage Characteristics in Organic Solar Cells Containing a TiOx Inter layer with Impedance Spectroscopy and Equivalent Circuit Analysis. *J. Phys. Chem. C* **2012**, *116*, 16333−16337.
(27) Wang, J. C.; Ren, X. C.; Shi, S. Q.; Leung, C. W.; Chan, P. K. L. Charge Accumulation Induced S-Shape *J*−*V* Curves in Bilayer Heterojunction Organic Solar Cells. *Org. Electron.* **2011**, *12*, 880−885.
(28) Wagenpfahl, A.; Rauh, D.; Binder, M.; Deibel, C.; Dyakonov, V. S-Shaped Current−Voltage Characteristics of Organic Solar Devices. *Phys. Rev. B* **2010**, *82*, 115306.
(29) Kumar, A.; Sista, S.; Yang, Y. Dipole Induced Anomalous S-Shape *I*−*V* Curves in Polymer Solar Cells. *J. Appl. Phys.* **2009**, *105*, 094512.
(30) Mor, G. K.; Jones, D.; Le, T. P.; Shang, Z.; Weathers, P. J.; Woltermann, M. K. B.; Vakhshouri, K.; Williams, B. P.; Tohran, S. A.; Saito, T.; Verduzco, R.; Salleo, A.; Hickner, M. A.; Gomez, E. D. Contact Doping with Sub-Monolayers of Strong Polyelectrolytes for Organic Photovoltaics. *Adv. Energy Mater.* **2014**, *4*, 1400439.
(31) Kim, S.; Park, M. J.; Balsara, N. P.; Liu, G.; Minor, A. M. Minimization of Focused Ion Beam Damage in Nanostructured Polymer Thin Films. *Ultramicroscopy* **2011**, *111*, 191−199.
(32) Park, M. J.; Kim, S.; Minor, A. M.; Hexemer, A.; Bolsara, N. P. Control of Domain Orientation in Block Copolymer Electrolyte Membranes at the Interface with Humid Air. *Adv. Mater.* **2009**, *21*, 203−208.
(33) Kozub, D. R.; Vakhshouri, K.; Orme, L. M.; Wang, C.; Hexemer, A.; Gomez, E. D. Polymer Crystallization of Partially Miscible Polythiophene/Fullerene Mixtures Controls Morphology. *Macromolecules* **2011**, *44*, 5722−5726.
(34) Vajjala Kesava, S.; Dhanker, R.; Kozub, D. R.; Vakhshouri, K.; Choi, U. H.; Colby, R. H.; Wang, C.; Hexemer, A.; Giebink, N. C.; Gomez, E. D. Mesoscopic Structural Length Scales in P3HT/PCBM Mixtures Remain Invariant for Various Processing Conditions. *Chem. Mater.* **2013**, *25*, 2812−2818.
(35) Guo, C.; Kozub, D. R.; Kesava, S. V.; Wang, C.; Hexemer, A.; Gomez, E. D. Signatures of Multiphase Formation in the Active Layer of Organic Solar Cells from Resonant Soft X-ray Scattering. *ACS Macro Lett.* **2013**, *2*, 185−189.
(36) NIST X-ray Photoelectron Spectroscopy Database. http://srdata.nist.gov/xps (accessed May 20, 2014).
(37) Treat, N. D.; Varotto, A.; Takacs, C. J.; Batara, N.; Al-Hashimi, M.; Heeney, M. J.; Heeger, A. J.; Wudl, F.; Hawker, C. J.; Chabinyc, M. L. Polymer−Fullerene Miscibility: A Metric for Screening New Materials for High-Performance Organic Solar Cells. *J. Am. Chem. Soc.* **2012**, *134*, 15869−15879.
(38) Parmer, J. E.; Mayer, A. C.; Hardin, B. E.; Scully, S. R.; McGehee, M. D.; Heeney, M.; McCulloch, I. Organic Bulk Heterojunction Solar Cells using Poly(2,5-bis(3-tetradecyllthiophen-2-yl)thieno[3,2,-b]thiophene. *Appl. Phys. Lett.* **2008**, *92*, 113309.
(39) Kim, J. Y.; Lee, K.; Coates, N. E.; Moses, D.; Nguyen, T. Q.; Dante, M.; Heeger, A. J. Efficient Tandem Polymer Solar Cells Fabricated by All-Solution Processing. *Science* **2007**, *317*, 222−225.
(40) Ali, A.; Madan, H. S.; Kirk, A. P.; Zhao, D. A.; Mourey, D. A.; Hudait, M. K.; Wallace, R. M.; Jackson, T. N.; Bennett, B. R.; Boos, J. B.; Datta, S. Fermi Level Unpinning of GaSb (100) Using Plasma Enhanced Atomic Layer Deposition of Al_2O_3. *Appl. Phys. Lett.* **2010**, *97*, 143502.
(41) Kozub, D. R.; Vakhshouri, K.; Kesava, S. V.; Wang, C.; Hexemer, A.; Gomez, E. D. Direct Measurements of Exciton Diffusion Length Limitations on Organic Solar Cell Performance. *Chem. Commun.* **2012**, *48*, 5859−5861.